The helical motions of roots are linked to avoidance of particle forces in soil

Adalvan Martins, Felicity O'callaghan, a Glyn Glyn Bengough, Kenneth Loades, Moacir Pasqual, Evelyne Kolb, Lionel Dupuy

The helical motions of roots are linked to avoidance of particle forces in soil

Adalvan Martins [1,2*], Felicity O'Callaghan[1], A Glyn Bengough[1,3], Kenneth W Loades[1], Moacir Pasqual[2], Evelyne Kolb[4], Lionel X. Dupuy[1*+]

[1] The James Hutton Institute, Invergowrie, DD25DA, Dundee, United Kingdom

[2] Federal University of Lavras, CP 3037, Lavras, MG, 37.200-000, Brazil

[3] School of Science and Engineering, University of Dundee, DD1 4HN, Dundee, United Kingdom

[4] Physics and Mechanics of Heterogeneous Materials (PMMH) Joint Research Program, Centre National de la Recherche Scientifique (CNRS, UMR 7636), Ecole Supérieure de Physique et Chimie Industrielle de Paris (ESPCI), Paris Sciences et Lettres Research University (PSL), Sorbonne Université - UPMC, Université Paris 06, Université Paris 07, 75005 Paris, France

[*] Equally contributing authors

[+] lionel.dupuy@hutton.ac.uk, +44 1382 568 815

Total word count for main text: 5131

Abstract: 160

Introduction: 599

Material and methods: 1683

Results: 1156

Discussion: 1836

Acknowledgments: 97

Abstract

- Limitation to root growth results from forces required to overcome soil resistance to deformation. The variations in individual particle forces affects root development and often deflects the growth trajectory.
- We have developed Transparent Soil and Optical Projection Tomography microscopy systems where measurements of growth trajectory and particle forces can be acquired in a granular medium at a range of confining pressures. We developed image processing pipelines to analyse patterns in root trajectories and a stochastic-mechanical theory to establish how root deflections relate to particle forces and thickening of the root.
- Root thickening compensates for the increase in mean particle forces but does not prevent deflections from 5% of most extreme individual particle forces causing root deflection. The magnitude of deflections increases with pressure but assemble into helices of conserved wavelength in a response linked to gravitropism.
- The study revealed mechanisms for the understanding of root growth in mechanically impeding soil conditions and provides insights relevant to breeding of drought-resistant crops.

Keywords

Biophysics, root, granular, mechanical stress, deflection, Transparent Soil

Introduction

To improve crop water and nutrient efficiency of crops, significant plant breeding interest is now focused on modifying the architecture of the root system to improve rooting depth (Lynch, 2011). Much of the attention is given to genetically controlling rooting angles to enhance drought resistance (Uga *et al.*, 2013) or to enhance nutrient acquisition (Liao *et al.*, 2001). While most crop research takes molecular genetics approaches to study the development of root system architectures, limitations arise because suitable traits for deep rooting are difficult to identify.

There is consequently a growing interest in understanding the biomechanical factors that limit root growth through soil (Colombi *et al.*, 2017b). Physical limitations to tissue expansion are linked to the physiology of the cell, in particular the cells ability to sustain turgor pressure and to soften the properties of cell walls (Mirabet *et al.*, 2011). Turgor pressure results in the build-up of tension forces within cell walls and growth occurs because the network of cellulose microfibrils permit extension and rearrangement (Braidwood *et al.*, 2014) through a mechanism termed polymer creep. Although the extensibility of primary cell walls is biochemically controlled (through pH, production of enzymes and free radicals, Cosgrove, 2005), growth can be mechanically arrested because external pressure exceeds turgor pressure, as initially shown by early biophysicists (Green *et al.*, 1971) and later studies (Geitmann & Ortega, 2009).

This view of the biophysics of growth is challenged in soils where plant roots grow under considerable levels of external pressure from an inhomogeneous soil medium. Turgor pressure in plant cells is rarely measured above 1 MPa, even when growth has been arrested (Meshcheryakov *et al.*, 1992; Clark *et al.*, 1996). This level of pressure corresponds well to the maximum axial pressure a root can exert on a rigid obstacle (Misra *et al.*, 1986) but not to the soil penetrometer pressure at which growth is arrested (5 MPa). Differences are attributed to lubrication by border cells, or flexibility of the root tissue (Bengough & Mullins, 1990). Still, turgor pressure within root cells is an order of magnitude less than known physiological limits of turgor, for example in fungal appressoria where turgor pressure can exceed 10 MPa (Howard *et al.*, 1991). Turgor pressure itself may not be the basis for limitation to deep rooting, and it is

reasonable to question why plants are not generating larger growth forces to penetrate hard soils.

The inhomogeneity of soil makes it difficult to understand the forces experienced by roots. Soils are comprised of particles held together by forces at the contact points between adjacent particles (repulsion, friction, cohesion). Even when dry and monodisperse, packings of particles are disordered (Majmudar & Behringer, 2005). Large variations in particle forces arise because of the heterogeneous distribution of contact points between particles, with the tail of the probability distribution of particle forces following an exponential distribution (Radjai *et al.*, 1998). It is not clear how such a stochastic distribution of forces will affect the growth of a root. The mechanics of root penetration has been the subject of recent computational studies (Fakih *et al.*, 2019), but conceptual frameworks to understand the nature of root responses to granular forces are still lacking.

We report here an analysis of microscale deflections of growth due to interactions with the soil granular structure. We develop an experimental system that captures the statistical distribution of particle forces exerted on the root and analyse growth responses to these forces. We propose a theory that links root elongation to particle force and show that root responses to mechanical interactions with particles are linked to the statistical distribution of these forces.

Materials and methods

Transparent Soils. Transparent Soil is a soil surrogate made of Nafion™, a transparent low refractive index polymer. It was prepared as described in (Downie *et al.*, 2012). Nafion pellets (4 mm×3 mm NR50 1100, Ion Power Inc., USA) were freezer milled and sieved with 1250 µm and 250 µm mesh size and polydispersity further characterised by image analysis (Methods S1-1). Particles were immersed in stock solutions of Hoagland No 2 basal solution (H2395, Sigma, USA) to adjust the pH and titrate the particles with mineral ions. These were shaken at 30°C for 30 minutes before replacing the nutrient solution (Downie *et al.*, 2012), and the operation was repeated until the pH was 6.5. The particles were rinsed with dH_2O to remove excess Hoagland media and autoclaved in dH_2O at 30% water content. The resulting particles had sizes ranging from 0.20 to 2.21 mm (Figure 1A).

Pressure chambers. Chambers were made of Sterilin™ Quickstart Universal Polystyrene 30mL tubes, and the piston applying the force at the surface of the soil was made of Sterilin™ Polystyrene 7 mL tubes (Methods S1-2). The piston was transparent to allow penetration of light and fitted with negligible friction with the inner wall of the chamber. A 3 mm hole was drilled in the cap of the inner tube (piston) to introduce the seed or the penetrometer needle for measuring penetration resistance forces. Compression in the chamber was applied by moving the base of the stage (Methods S1-2) and monitoring soil confining pressure with a 20 N load cell (Applied Measurements Ltd). The intensities of the compression applied to the soil were 0 N (0 kPa, control), 10 N (25 kPa) and 20 N (50 kPa).

Resistance to penetration. Penetrometer resistance was measured within chambers under confining pressure of 0 kPa, 25 kPa and 50 kPa (n=6). Penetrometer resistance was measured using an Instron 5544 universal test frame (Instron, MA, USA) fitted with a 50 N load cell accurate to ±2 mN (Methods S1-3). The penetrometer needle used was a cone shaped tip of 30^o semiangle with a base of 1.72 mm in diameter and a cross-sectional area of 2.32 mm^2 and a 20% rebated shaft to minimise shaft friction. Shaft cones of 30^o semiangle are commonly used as root analogues because they compromise well between cone friction and formation of soil bodies (Bengough & Mullins, 1990). Crosshead displacement for penetrometer testing was performed at a rate of 2 mm min^{-1} to maintain quasi-static conditions (Methods S1-2). It has been shown experimentally that dynamic effects are observed for penetration rates that are one or two orders of magnitude larger (Bengough & Mullins, 1990). Depths of 20 to 40 mm were tested because the mean force was approximately constant over this range and shaft friction negligible. We define the particle force F_i as the i^{th} peak of force recorded in this experiment. Mean force $\langle F \rangle$, third quartile $F_{75\%}$, and probability distribution of particle forces were characterised.

Root biomechanics. The mechanical resistance of seedling roots (n=7) was tested under compression. Seeds were germinated using germination paper until the roots were approximately 2 cm long. Seedling primary roots were then anchored in plaster of Paris and tested under axial compression (Methods S1-3) using an Instron 5544 universal test frame as described above.

Plant growth. Lentil (*Lens culinaris*) cv. Peridot seeds were sterilised in 10% solution of sodium hypochlorite for 20 minutes. Seeds were pre-germinated on germination paper at 25°C and photoperiod of 16 h. After root protrusion (36 h), the seeds were transferred to a cylindrical chamber containing Transparent Soil held at 30% volumetric water content. The germinated seeds grew for 3 days at 25°C in soil maintained at 0 kPa, 25 kPa and 50 kPa of confining pressure (n=5). Roots were then washed and digitally scanned with root diameter measured along the first 2 cm of the root from the apical meristem.

3D Microscopy. After 3 days of growth, a solution of 20% trehalose was added for refractive index matching with the soil particles. A vacuum pump (RelChron PPROB-10398) was used to remove air bubbles present in the samples. Images were collected 15 hours after the addition of trehalose under laboratory conditions with an Optical Projection Tomography microscope (Sharpe *et al.*, 2002). The microscope was made from a Leica MZ16 FA stereomicroscope fitted with a 0.5X plan achromatic objective for long working distance (135 mm) and a Leica DFC350FX camera (Figure 1B). Each scan consisted of 720 projections taken every 0.5 degree. Scans were obtained at three different depths and achieved 13 to 20 µm resolution and 3 cm field of view out of 5 cm of soil depth. The image data obtained from three different depths were combined using Fiji sequence stitching (Schindelin *et al.*, 2012), and 3D reconstructions were performed in Matlab (MathWorks Inc.) using the filtered backprojection algorithm. Confocal laser scanning imaging was done on a Nikon A1R microscope. Roots were stained with calcofluor (fluorescent brightener 28; Sigma F3543) and imaged using either x4 or x10 magnification.

Signal processing. We developed a pipeline to reconstruct the root centreline with precision (Figure 2A). First, a 3D vessel tracing algorithm was used to obtain a coarse representation of the root centreline (Friman *et al.*, 2010). To improve the accuracy and precision of the root centreline a multiplane tracing approach was developed (Methods S2-1) by generalisation of bi-plane snakes (Canero *et al.*, 2000). Root centrelines were subsequently centred along the z-axis. This was achieved using a spline regression with 3 anchor points and fitted values were subtracted from the original signal. Centred signals $f(t)$ were then analysed for helical patterns. The analysis was based on a modification of the Fourier transform to include orthonormal helix forming basis functions (Figure 2B),

$$\psi_0(t) = \left(0,0,\sqrt{3}t\right) \text{ and } \psi_k(t) = (e^{i2\pi kt}, e^{i(2\pi kt-\pi/2)}, 0), \quad (1)$$
$$k\,\epsilon[-N,N].$$

171 t represents the rooting depth and k the spatial frequency. The sign of k indicates
172 clockwise or anti-clockwise helices. The coefficients of the transform C_k are then
173 obtained by projection on the set of basis functions,

$$C_k = \int_0^T (f_x;\ f_y;\ f_z/T^2) \cdot \overline{\psi_k} dt. \quad (2)$$

174 The wavelength of the helix is $\lambda_k = |1/k|$. $\tilde{\lambda}_k$ is the length of root contained in a helix
175 of one period is therefore

$$\tilde{\lambda}_k = \sqrt{1 + (2\pi k r_k)^2}\lambda_k, \quad (3)$$

176 where $r_k = \sqrt{C_k\overline{C_k}} + \sqrt{C_{-k}\overline{C_{-k}}}$ is the radius of the waveform of frequency k. We also
177 introduce the asymmetry ratio R_a,

$$R_a = \frac{C_{-j}\overline{C_{-J}}}{C_k\overline{C_k}} \quad (4)$$

178 where k>0 and j>0 are respectively the clockwise and anticlockwise dominant
179 frequencies of opposite sense of rotation. The asymmetry ratio $0 \leq R_a \leq 1$ indicates
180 whether the helix change its sense of rotation during growth. When clockwise and
181 anticlockwise spectra have identical peaks, R_a is equal to 1, and in the case of a perfect
182 helix of infinite length, it is equal to 0. When analysing real data, extremal values are
183 not reached but relative values of R_a indicate the degree of consistency of the sense
184 of rotation of a root helical trajectory. Changes in root directions were identified as
185 local maxima in the root curvature. A custom software RootHix was developed to
186 perform the analyses (www.archiroot.org.uk/tools.html). Full mathematical derivation
187 of the analysis can be found in Methods S2-2. The data generated in this study is
188 available for download on the following Zenodo repository
189 https://zenodo.org/record/889946#.WbgwrsiGO-4.

190 **Theory for root-particle interactions.** Root deflection occurs when the energy of
191 axial elongation U_e becomes larger than the energy U_b required for bending and lateral
192 displacement of particles (Figure 2C),

$$U_b(E, I, \langle F \rangle, d, \delta) < U_e(F, \delta). \quad (5)$$

F (N) is the force required to displace the particle in front of the root, E (Pa) is the Young's modulus of the root tissue, I (m^4) is the second moment of area of the root, $\langle F \rangle$ is the mean particle force, δ is the mean displacement between two peak forces in a penetrometer test, and d is the distance between particles determined as the mean particle diameter (Methods S3).

Since U_e is a growing function of F, it is possible to calculate from equation 5 a critical force F_{crit} above which the deflection of the root will occur,

$$F_{crit} = A(EI)^{1/4}\langle F \rangle^{3/4} d^{1/2}\delta^{-1}, \quad (6)$$

with a bending constant $A \approx 0.237$. A similar calculation can be made if the tissue has viscoelastic properties. In this case, E is replaced with a time-dependent coefficient $E^*(t)$, termed creep function, which we obtain from the Kelvin Voigt viscoelastic model,

$$\frac{1}{E^*(t)} = \frac{1}{E}\left(1 - \exp -\frac{E}{\eta}t\right). \quad (7)$$

t here refers to the time required for the root growth to overcome a particle and is determined as d/v where v is the root tip velocity (m s^{-1}). The probability of a deflection occurring can then be expressed from the distribution of particle forces obtained from penetrometer test. Because deflections are rare, they must be caused by large particle forces which occurrence is described by the tail of the distributions of particle forces. These follow an exponential law,

$$q = \frac{1}{4}\exp[-b(F_{crit} - F_{75\%})]. \quad (8)$$

The theory then provides the probability distribution (pdf) σ and κ of the occurrence of deflections and curvature of the root respectively,

$$\sigma(x) = \frac{q}{\delta}\exp\left(-\frac{xq}{\delta}\right), \quad (9)$$

$$\kappa(x) = \frac{q^2 d^2}{\langle l \rangle^2 \delta^2 x^3}\exp\left(-\frac{qd}{\langle l \rangle \delta x}\right). \quad (10)$$

$\langle l \rangle = B(d^2 EI/\langle F \rangle)^{\frac{1}{4}}$ is the expected bending length with $B \approx 2.06$. The pdf of root curvature follows an inverse gamma distribution with shape parameter 2 and scale

parameter $qd/\langle l\rangle\delta$. Full mathematical derivation for models can be found in Methods S3.

When the tissue is anisotropic, root reorientation occurs preferentially along a given axis of rotation (blue cone, Figure 2D). The axis of rotation defines two equally probable bending directions V_1 and V_2. Because the anisotropy is helical, V_1 and V_2 are not constant but rotate along the roots (red arrow, Figure 2D). To test whether deflections occur preferentially in certain directions, we assign the probability q_1 for direction V_1 and $q_2 = 1 - q_1$ for V_2. We used equations 5-8 to simulate the occurrence of deflections in an elongating root based on experimental data and assumed three scenarios for the direction of deflection. If the deflection has no predefined direction (random deflection) then $q_1 = q_2 = 0.5$. If there is an intrinsic sense of rotation then $q_1 = 1$ or $q_2 = 1$. If the direction of deflection occurs preferentially towards gravity (gravitropic deflection), the probability is

$$q_1 = \frac{\tanh(-G\Delta\alpha) + 1}{2} \tag{11}$$

$\Delta\alpha = \alpha_1 - \alpha_2$ is the difference in verticality between V_1 and V_2, i.e. α_1 (respectively α_2) is the positive angle between V_1 (respectively V_2) and the downward vertical. G defines the sensitivity of the response to gravity.

Results

Resistance to penetration. Penetrometer tests produced stochastic data (Figure 3A). Analysis of the data showed soil confining pressure (0 kPa, 25 kPa, and 50 kPa, generated by loads of 0 N, 10 N and 20 N respectively) increased the mean penetration force. In soils that were not held under compression, the mechanical resistance to penetration was the lowest with $\langle F\rangle = 0.15$ N (± 0.01), $F_{75\%} = 0.19$ N. In soils held under a confining pressure of 25 kPa, the resistance to penetration increased to $\langle F\rangle = 1.11$ N (± 0.03), $F_{75\%} = 1.18$ N. The highest resistance to penetration, $\langle F\rangle = 2.14$ N (± 0.03), $F_{75\%} = 2.26$ N, was obtained in soils held at a confining pressure of 50 kPa (Figure 3B).

We analysed the sequence of forces recorded during penetration (Figure 3C&D). The tail of the statistical distribution of transformed particle forces (Figure 3C) showed an exponential decline, with characteristic force values ($1/b$) measured as 36.3 mN, 75.9

mN and 95.3 mN for respectively 0 kPa, 25 kPa and 50 kPa of soil confining pressure. Permutation tests showed the exponential tail of the distribution was not affected by the increase in confining pressure from 25 kPa to 50 kPa ($p=0.88$), but there was a statistical difference between uncompressed and compressed soils ($p<0.001$).

We also studied the distances δ between peak forces (Figure 3D). The probability density of δ followed an exponential decline with a characteristic distance of 0.13 mm. No statistical differences were found between soils under compression ($p=0.94$) nor between compressed and uncompressed soil ($p=0.12$). The distance between the peaks of force was substantially smaller than the size of the particle diameter (1 mm on average).

Roots helical response to mechanical forces. Plant roots grew healthily in all experiments (Figure 4A). Soil confining pressure reduced root elongation rates and increased root diameters. Roots growing in soil without confining pressure exhibited the fastest elongation rate of 1.99 $cm.d^{-1}$ (±0.40) and had diameters of 0.64 mm (±0.04) at 2 cm from the root tip. Roots growing in soil under 25 kPa of confining pressure exhibited an elongation rate of 1.60 $cm.d^{-1}$ (±0.42) and had diameters of 0.69 mm (±0.03). Roots growing in soil under 50 kPa of confining pressure exhibited an elongation rate of 1.36 $cm.d^{-1}$ (±0.28) and had diameters of 0.75 mm (±0.07).

Root centrelines exhibited helical morphologies (Figure 4A) which could be detected by helical transformation (Figure 4B). The analysis identified a dominant wavelength that is not affected by soil confining pressure. Wavelength values ($\tilde{\lambda}$) were 13.7 mm (±1.4), 12.1 mm (±0.5) and 12.8 mm (±0.6) for pressures of 0 kPa, 25 kPa and 50 kPa respectively (Figure 4C). However, the radius of the helix r_k r_k significantly increased from 0.17 mm (±0.03), to 0.24 mm (±0.03) and 0.30 mm (±0.04) for pressures of 0 kPa, 25 kPa and 50 kPa. These helical shapes had curvatures of respectively 0.034 mm^{-1}, 0.063 mm^{-1} and 0.071 mm^{-1}. Helices were clockwise, anti-clockwise and occasionally changed direction of rotation along the same root axis.

Compression tests were used to characterise the mechanical properties of roots (Figure 4D). All roots tested deformed into a helical shape at an average force of 20.0 mN (±1.5). Helical shapes were more pronounced near the tip where the root was thinner. Roots retained their helical shape after removal of the axial forces. The wavelength of the helix ($\tilde{\lambda}$ =12.2 mm ± 2.0) closely matched those measured in Transparent Soil, but

the radius of the helix (0.9 mm ± 0.1) was about three times as large as the value measured under 50 kPa of confining pressure. The mechanical test was interrupted before roots were visibly fractured. Roots were subsequently moved into water and recovered their shape within 20 minutes.

Soil particles influence root deflections. Roots curvatures at deflections exceeded those of fitted helices by an order of magnitude (Figure 5A). The distance between the sites of deflections was not influenced by the pressure acting on the soil. The distribution of the distance between the sites of two successive deflections was approximately uniform, with distances spanning between 500 µm and 6 mm with an average of 2.5 mm (Figure 5B). Since the characteristic distance between peaks of forces produced by soil particles is δ = 0.13 mm and one deflection occurs every 2.5 mm of root growth in average, thus 5% of particle force events produced root deflections.

The curvature of the root where deflection occurs was influenced by soil confining pressure (Figure 5C). In the absence of confining pressure, curvatures were below 0.2 mm^{-1}. When 25 kPa of pressure was applied, curvatures measured were below 0.3 mm^{-1}, whereas when 50 kPa of pressure was applied, curvatures above 0.4 mm^{-1} were measured. Confocal laser scanning microscopy observations showed sharp deflections extending over a length of root of around 700 µm. The curvature of these deflections increased with increases in confining pressure. There was little evidence of tissue torsion. Angle in the files of epidermal cells relative to the local longitudinal root axis was rarely observed and did not correlate with the sites of deflection (Figure 5C Inset).

Linking root gravitropism and deflections to helix formation. The model described the overall root responses to confining pressure for the distribution of curvatures (Figure 6A Top) but overestimated the deflection in the high frequency domain (Figure 6A Middle) . The Young's modulus required to predict the range of curvatures varied between 1.5 and 5.0 MPa (3.7 MPa ±1.4, 1.64 MPa ±0.62 and 2.05 MPa ±0.78 for respectively 0 kPa, 25 kPa and 50 kPa of confining pressure) and declined with confining pressure (Figure 6A Bottom). Apparent variations in the Young's modulus may be due to the viscoelasticity of the tissue, with Kelvin Voigt model best fitting data with $E = 21.5$ kPa and $\eta = 1.7$ GPa. s.

There was strong evidence of the role of gravitropism in the maintenance of helical shapes. Experimental results showed the asymmetry ratio R_a is decreasing linearly with root deviation from verticality (black curves, Figure 6B top right). Roots that grew more horizontally had therefore a greater tendency to maintain a consistent helix and conserved sense of rotation. Simulations demonstrated this is caused by a bias in the direction of growth when a deflection occurs. When random deflections were imposed in the simulations (red curves, Figure 6B), roots lost their ability to maintain helical forms due to the sense of rotation of the helix changing randomly when hitting an obstacle: R_a was larger than in all other cases and also independent of the deviation from verticality. Roots which deflected following a fixed direction V_1 or V_2 (green curves, Figure 6B) naturally produced helix with unchanged sense of rotation (asymmetry ratio ≈0.3). Here too, the model could not predict the experimental effect of deviation from verticality on the asymmetry ratio. Roots which direction of deflection was influenced by root verticality (gravitropic simulation, Figure 6B, blue curve) produced more realistic growth patterns and induced the formation of helices with occasional switches in the sense of rotation, but these switches were less frequent.

Discussion

Linking root responses to soil structure. Biophysical theories link growth response to soil pressure, cell wall rheology, and water potential (Greacen & Oh, 1972; Dexter, 1987). If the soil pressure on the root and the tensile stresses in the cell walls exceed turgor pressure, then growth must be arrested (Plant, 1982; Dexter, 1987). Our approach departs from this view and links root physical limitations to the mechanical stability and deflections of the root tip due to surrounding particle forces. Therefore, critical root elongation forces define the ability of a root to remain mechanically stable, and this ability is linked to the rigidity of the tissue and the distribution of particle forces.

The emergence of theories for the prediction of critical elongation forces has been largely limited by the ability to characterise the mechanical environment of a growing root. Experimental systems using compression chambers of various sorts have been extensively used in the 1960's and later (Barley, 1962; Materechera *et al.*, 1991; Abdalla A *et al.*, 1969), but simultaneous measurements of particle forces were not

made. The first attempts of Whiteley and Dexter (1982) showed measuring the drag force of a particle of known size and traction speed is possible but precise control of particle displacement is not. More recently, research on the physics of granular media has characterised interparticle mechanics using planar force sensors or computational methods (Mueth *et al.*, 1998; Hurley *et al.*, 2016), but application of such techniques within biological systems remains difficult. Use of photo-elastic materials has been successful (Kolb *et al.*, 2012; Wendell *et al.*, 2012) but current materials do not allow fabrication of realistic soil-like substrate, and for this reason, penetrometer resistance tests remain the preferred approach to characterise the resistance to root elongation (Clark *et al.*, 2003). Root responses to particle forces are equally difficult to monitor. Particle displacements have been measured alongside root deflections in glass bead substrates using tracking algorithms (Bengough *et al.,* 2009). More recently X-ray computed tomography has achieved similar results in 3D (Keyes *et al.*, 2017). Deriving measurements of forces from such data is not currently possible because it would require detection of the deformation of individual particles (Brodu *et al.*, 2015).

In this study we have addressed some of these challenges and characterised how root deflections occur in relation to the distribution of particle forces in the growth medium. Our pressure chamber shares similarity with the system used by (Materechera *et al.*, 1991), but we additionally monitored 3D growth trajectories and measured penetrometer resistance. More importantly, we have developed signal processing technologies to retrieve the wavelength and radius of root helices and to study the frequency and magnitude of root deflections, e.g. using multiplane tracing and helical transform (Figure 2 A&B). Previously, few studies have utilised the variations observed in penetration resistance. Geostatistical tools were used to analyse periodic variation in penetration resistance in relation to changes in soil structure (Grant *et al.*, 1985; Hadas & Shmulewich, 1990), but none of these studies linked variations in particle forces to growth trajectories and root responses to mechanical stress.

Theory for growth in confined soil environments. Using our experimental system, it was possible to identify factors that heavily influence root responses to interactions with soil particles.

Granular media appear to cause frequent deflections of the root trajectory. Growth response to soil heterogeneity has been widely documented (Goss & Russell, 1980),

and can be commonly observed in the form of tortuous morphologies, for example in compacted soil (Popova *et al.*, 2016). Our results showed the presence of root deflections appears to be independent of soil mechanical resistance and may prevail in granular media. Deflections occur by bending at the root tip as observed on other root species (Bizet *et al.*, 2016), and it is predominantly the magnitude of deflection, not the frequency, that is affected by soil confining pressure (Figure 5). The study was limited to roots and particles within a narrow range of sizes. It is unclear how the mechanisms described here translate across spatial scales. Root behaviours in finer or cohesive soils are notable. Arguably, some degree of homogenisation of particle forces would apply (Kolb *et al.*, 2017), but granular media are also known to exhibit macroscopic behaviour such as arching or clustering (Delenne *et al.*, 2004; Aranson & Tsimring, 2006). Therefore, root trajectories in these conditions may also exhibit sequences of deflections that are similar to those observed in our study.

Root deflections are linked to a mechanical process controlled by the fluctuations of particle forces acting at the root tip. We have characterised the nature of particle forces and found patterns that confirm this hypothesis. The distance between peak particle forces (δ) is conserved across a range of confining pressures, and the tail of the statistical distribution of particle forces experienced by a root is exponential, as is commonly found in granular media (Figure 3C, Radjai *et al.*, 1998). Because the distance between the sites of deflections is larger than δ and larger than the size of particles (Figure 5B), we conclude that in our experimental set-up, a root can often displace soil particles axially, but that on rare occasions the growth trajectory is deflected. Deflection also requires mechanical energy to bend the root and displace particles laterally (Gordon *et al.*, 1992), and therefore it is both the distribution of axial and lateral particle forces that determine if a deflection will take place.

Root deflections are mechanically viscoelastic and anisotropic, and may be influenced by gravitropism. Results show roots did not fully recover their shape following mechanical tests (Figure 4D). Also, there was time dependence of the apparent Young's modulus determined experimentally from the model (Figure 6A). This behaviour is typical of viscoelastic materials (Findley & Davis, 2013). Since the time required to overcome a soil particle (between 9 and 14 minutes) exceeds the duration of mechanical testing, visco-elastic deformation must affect the nature of the deflection. This is also consistent with the requirements for tissues to elongate

(Braidwood *et al.*, 2014) and for fluids to move across cells (Nonami *et al.*, 1997). We observed the formation of helices with wavelengths similar to those observed during the waving phenomenon observed at the surface of agar (Rutherford *et al.*, 1998). The curvature of helices is an order of magnitude smaller than the curvature at the sites of a deflection and we conclude helical shapes are due to the combined anisotropy of the tissue (Lloyd & Chan, 2002) and the frequency of deflections. Unlike what was proposed by Silverberg *et al.* (2012), torsion pre-stress is not required for helices to form.

We have formalised the conditions for the occurrence of a deflection. Our theory predicts how roots respond to soil confining pressure in granular media, and it shows that roots deflect at frequencies that are maintained across increasing levels of soil confining pressure (Figure 5B). This is counterintuitive because the forces required to displace soil particles are increasing too. However, root thickening and subsequent stiffening of the tissue (Materechera *et al.*, 1991; Bengough *et al.*, 2006) prevent the increase in frequency of deflections. The thickening is not sufficient to limit the magnitude of deflections which, as predicted by the mechanics of embedded structures (Mojdehi *et al.*, 2016), results in shorter bending length and increased curvature (Popova *et al.*, 2016).

Our theory also showed limitations. The mean field approximation used to establish the critical particle force led to oversimplified predictions of distances between deflections (Figure 6A). The model itself did not address either how the soil structure or the displacement of particles affects the stochasticity of forces. However, various experimental and theoretical studies are now addressing these limitations. The stochasticity of soil penetrometer resistance is now being linked to soil structure (Ruiz *et al.*, 2017). Theoretical work on snow mechanics has also successfully demonstrated how understanding the microstructure of a granular media can lead to improved predictions of forces applied on a penetrating structure (Schneebeli *et al.*, 1999; Löwe & van Herwijnen, 2012). In the future, our theory could therefore be improved by better accounting for variations in particle forces, and this could allow prediction of root growth and morphology to be made directly from the knowledge of soil structure.

Root navigation through paths of least resistance in soil. Roots are known to mobilise various sensing mechanisms in response to obstacles. For example, response

435 to touching an obstacle has been found to mobilise also gravity sensing (Massa &
436 Gilroy, 2003) and the root cap is believed to play a key role in the reorientation of the
437 tip. Skewing and waving patterns observed during growth on gels are also thought to
438 result from gravitropism and touch stimuli (Migliaccio & Piconese, 2001; Oliva &
439 Dunand, 2007). Similar mechanisms also prevail in the field where roots are known
440 for example to grow in macropores (Moran *et al.*, 2000; White & Kirkegaard, 2010).
441 The phenomenon was recently found, for example, to compensate for the effects of
442 soil compaction (Colombi *et al.*, 2017a).

443 In this study we found evidence that root responses to soil pressure results from
444 interactions taking place at the level of the soil particle. Helical shapes were formed
445 more consistently when roots deviated from verticality (Figure 6B), and this was due
446 to gravitropic effects during deflections from particles. Simulations predicted smaller
447 asymmetry ratio than those measured experimentally (Figure 6B) , which indicates
448 that simulated root morphologies are more helical. This could be explained by
449 constraints imposed in the model on the direction of deflections. The model did not
450 include biological responses linked to the anisotropy of the tissue either. For example,
451 we did not include changes in the mechanical properties of the tissue in response to
452 gravitropic stimulation. Such responses were not studied experimentally here, but
453 work on *Arabidopsis thaliana* have shown that a number of biomechanical factors can
454 affect the waving mechanism observed in roots (Buer *et al.*, 2003). Mechanical
455 properties of root tissues are also known to vary in response to mechanical stresses
456 and consequently to confining pressure (Loades *et al.*, 2013).

457 The conservation of the root deflection frequency also hints at a potential mechanism
458 for growth through paths of least resistance in soil. Because deflections limit exposure
459 to large particle forces, they reduce the overall resistance opposed to elongation.
460 Deflections have also undesirable consequences on root foraging dynamics. For
461 example, models predict that stochastic deflections result in a transition from a
462 convective to a dispersive propagation through soil (Dupuy *et al.*, 2018), and a
463 subsequent reduction in rooting depth.

464 The development of deep roots requires mechanical stability of elongating tissues.
465 Extreme pressures, deformations, or deflections of the root apex are known to affect
466 the cellular organisation of the meristem (Jackson *et al.*, 2017). In such conditions, the

developmental functions of the meristem may be affected, and the ability to explore new regions of soil or access resources may become limited. Some control of the morphological and structural properties of tissues in response to soil mechanical properties must therefore prevail. The way sensing of and response to the micromechanical environment operate, however, requires additional study.

Acknowledgments

ADM was funded by PDSE/CAPES (99999.006158/2015-03). LXD was supported by a consolidator fellowship from the European Research Council (ERC SENSOILS-647857). The James Hutton Institute receives support from the Scottish Government Rural and Environment Science and Analytical Services Division (RESAS, Workpackage 1.1.1,2.1.6,2.1.7,2.3.4). Collaborations were also greatly facilitated by the funding from the ROSOM project (Agropolis Foundation ID 1202-073, Labex Agro ANR-10-LABX-001-01) and the Chaire Joliot (LXD) of the ESPCI Paris, PSL Research University. We thank Joseph Alawi for assistance with processing of image data, Jean-Luc Maeght and Philip White for the fruitful discussions and comments on the manuscript.

Bibliography

Abdalla A, Hettiaratchi D, Reece A. 1969. The mechanics of root growth in granular media. *Journal of agricultural engineering research* **14**(3): 236-248.

Aranson IS, Tsimring LS. 2006. Patterns and collective behavior in granular media: Theoretical concepts. *Reviews of modern physics* **78**(2): 641.

Barley K. 1962. The effects of mechanical stress on the growth of roots. *Journal of Experimental Botany* **13**(1): 95-110.

Bengough AG, Bransby MF, Hans J, McKenna SJ, Roberts TJ, Valentine TA. 2006. Root responses to soil physical conditions; growth dynamics from field to cell. *Journal of Experimental Botany* **57**(2): 437-447.

Bengough AG, Hans J, Bransby MF, Valentine TA. 2009. PIV as a method for quantifying root cell growth and particle displacement in confocal images. *Microscopy Research and Technique* **73**(1): 27-36.

Bengough AG, Mullins CE. 1990. Mechanical impedance to root growth: a review of experimental techniques and root growth responses. *European Journal of Soil Science* **41**(3): 341-358.

Bizet F, Bengough AG, Hummel I, Bogeat-Triboulot M-B, Dupuy LX. 2016. 3D deformation field in growing plant roots reveals both mechanical and biological responses to axial mechanical forces. *Journal of Experimental Botany* **67**(19): 5605-5614.

Braidwood L, Breuer C, Sugimoto K. 2014. My body is a cage: mechanisms and modulation of plant cell growth. *New Phytologist* **201**(2): 388-402.

Brodu N, Dijksman JA, Behringer RP. 2015. Spanning the scales of granular materials through microscopic force imaging. *Nature communications* **6**: 6361.

Buer CS, Wasteneys GO, Masle J. 2003. Ethylene modulates root-wave responses in Arabidopsis. *Plant Physiology* **132**(2): 1085-1096.

Canero C, Radeva P, Toledo R, Villanueva JJ, Mauri J 2000. 3D curve reconstruction by biplane snakes. *Pattern Recognition, 2000. Proceedings. 15th International Conference on*: IEEE. 563-566.

Clark L, Whalley W, Dexter A, Barraclough P, Leigh R. 1996. Complete mechanical impedance increases the turgor of cells in the apex of pea roots. *Plant, Cell & Environment* **19**(9): 1099-1102.

Clark LJ, Whalley WR, Barraclough PB. 2003. How do roots penetrate strong soil? *Plant and Soil* **255**(1): 93-104.

Colombi T, Braun S, Keller T, Walter A. 2017a. Artificial macropores attract crop roots and enhance plant productivity on compacted soils. *Science of the Total Environment* **574**: 1283-1293.

Colombi T, Kirchgessner N, Walter A, Keller T. 2017b. Root tip shape governs root elongation rate under increased soil strength. *Plant Physiology* **174**(4): 2289-2301.

Cosgrove DJ. 2005. Growth of the plant cell wall. *Nature Reviews: Molecular Cell Biology* **6**(11): 850-861.

Delenne JY, El Youssoufi MS, Cherblanc F, Bénet JC. 2004. Mechanical behaviour and failure of cohesive granular materials. *International Journal for Numerical and Analytical Methods in Geomechanics* **28**(15): 1577-1594.

Dexter A. 1987. Mechanics of root growth. *Plant and Soil* **98**(3): 303-312.

Downie H, Holden N, Otten W, Spiers AJ, Valentine TA, Dupuy LX. 2012. Transparent soil for imaging the rhizosphere. *PloS One* **7**(9): e44276.

Dupuy LX, Mimault M, Patko D, Ladmiral V, Ameduri B, MacDonald MP, Ptashnyk M. 2018. Micromechanics of root development in soil. *Current Opinion in Genetics & Development* **51**: 18-25.

Fakih M, Delenne J-Y, Radjai F, Fourcaud T. 2019. Root growth and force chains in a granular soil. *Physical Review E* **99**(4): 042903.

Findley WN, Davis FA. 2013. *Creep and relaxation of nonlinear viscoelastic materials*: Courier Corporation.

Friman O, Hindennach M, Kühnel C, Peitgen H-O. 2010. Multiple hypothesis template tracking of small 3D vessel structures. *Medical Image Analysis* **14**(2): 160-171.

Geitmann A, Ortega JK. 2009. Mechanics and modeling of plant cell growth. *Trends in Plant Science* **14**(9): 467-478.

Gordon D, Hettiaratchi D, Bengough A, Young I. 1992. Non-destructive analysis of root growth in porous media. *Plant, Cell & Environment* **15**(1): 123-128.

Goss M, Russell RS. 1980. Effects of mechanical impedance on root growth in barley (*Hordeum vulgare* L.) III. Observations on the mechanism of response. *Journal of Experimental Botany* **31**(2): 577-588.

Grant C, Kay B, Groenevelt P, Kidd G, Thurtell G. 1985. Spectral analysis of micropenetrometer data to characterize soil structure. *Canadian Journal of Soil Science* **65**(4): 789-804.

Greacen E, Oh J. 1972. Physics of root growth. *Nature New Biology* **235**(53): 24.

Green P, B., Erickson RO, Buggy J. 1971. Metabolic and physical control of cell elongation rate. *Plant Physiology* **47**: 423-430.

Hadas A, Shmulewich I. 1990. Spectral analysis of cone penetrometer data for detecting spatial arrangement of soil clods. *Soil and Tillage Research* **18**(1): 47-62.

Howard RJ, Ferrari MA, Roach DH, Money NP. 1991. Penetration of hard substrates by a fungus employing enormous turgor pressures. *Proceedings of the National Academy of Sciences* **88**(24): 11281-11284.

Hurley RC, Hall SA, Andrade JE, Wright J. 2016. Quantifying interparticle forces and heterogeneity in 3D granular materials. *Physical Review Letters* **117**(9): 098005.

Jackson MD, Duran-Nebreda S, Bassel GW. 2017. Network-based approaches to quantify multicellular development. *Journal of The Royal Society Interface* **14**(135): 20170484.

Keyes SD, Cooper L, Duncan S, Koebernick N, McKay Fletcher DM, Scotson CP, van Veelen A, Sinclair I, Roose T. 2017. Measurement of micro-scale soil deformation around roots using four-dimensional synchrotron tomography and image correlation. *Journal of the Royal Society, Interface* **14**(136): 20170560.

Kolb E, Hartmann C, Genet P. 2012. Radial force development during root growth measured by photoelasticity. *Plant and Soil* **360**(1-2): 19-35.

Kolb E, Legué V, Bogeat-Triboulot M-B. 2017. Physical root–soil interactions. *Physical Biology* **14.6**: 065004.

Liao H, Rubio G, Yan X, Cao A, Brown KM, Lynch JP. 2001. Effect of phosphorus availability on basal root shallowness in common bean. *Plant and Soil* **232**(1-2): 69-79.

Lloyd C, Chan J. 2002. Helical microtubule arrays and spiral growth. *The Plant Cell* **14**(10): 2319-2324.

Loades K, Bengough A, Bransby M, Hallett P. 2013. Biomechanics of nodal, seminal and lateral roots of barley: effects of diameter, waterlogging and mechanical impedance. *Plant and Soil* **370**(1-2): 407-418.

Löwe H, van Herwijnen A. 2012. A Poisson shot noise model for micro-penetration of snow. *Cold Regions Science and Technology* **70**: 62-70.

Lynch JP. 2011. Root phenes for enhanced soil exploration and phosphorus acquisition: tools for future crops. *Plant Physiology* **156**(3): 1041-1049.

Majmudar TS, Behringer RP. 2005. Contact force measurements and stress-induced anisotropy in granular materials. *Nature* **435**(7045): 1079-1082.

Massa GD, Gilroy S. 2003. Touch modulates gravity sensing to regulate the growth of primary roots of *Arabidopsis thaliana*. *Plant Journal* **33**: 435-445.

Materechera S, Dexter A, Alston AM. 1991. Penetration of very strong soils by seedling roots of different plant species. *Plant and Soil* **135**(1): 31-41.

Meshcheryakov A, Steudle E, Komor E. 1992. Gradients of turgor, osmotic pressure, and water potential in the cortex of the hypocotyl of growing ricinus seedlings effects of the supply of water from the xylem and of solutes from the phloem. *Plant Physiology* **98**(3): 840-852.

Migliaccio F, Piconese S. 2001. Spiralizations and tropisms in *Arabidopsis* roots. *Trends in Plant Science* **6**(12): 561-565.

Mirabet V, Das P, Boudaoud A, Hamant O. 2011. The role of mechanical forces in plant morphogenesis. *Annual Review of Plant Biology* **62**: 365-385.

Misra R, Dexter A, Alston A. 1986. Maximum axial and radial growth pressures of plant roots. *Plant and Soil* **95**(3): 315-326.

Mojdehi AR, Tavakol B, Royston W, Dillard DA, Holmes DP. 2016. Buckling of elastic beams embedded in granular media. *Extreme Mechanics Letters* **9**: 237-244.

Moran CJ, Pierret A, Stevenson AW. 2000. X-ray absorption and phase contrast imaging to study the interplay between plant roots and soil structure. *Plant and Soil* **223**(1): 101-117.

Mueth DM, Jaeger HM, Nagel SR. 1998. Force distribution in a granular medium. *Physical Review E* **57**(3): 3164-3169.

Nonami H, Wu Y, Boyer JS. 1997. Decreased growth-induced water potential (a primary cause of growth inhibition at low water potentials). *Plant Physiology* **114**(2): 501-509.

Oliva M, Dunand C. 2007. Waving and skewing: how gravity and the surface of growth media affect root development in *Arabidopsis*. *New Phytologist* **176**(1): 37-43.

Plant RE. 1982. A continuum model for root growth. *Journal of Theoretical Biology* **98**(1): 45-59.

Popova L, van Dusschoten D, Nagel KA, Fiorani F, Mazzolai B. 2016. Plant root tortuosity: an indicator of root path formation in soil with different composition and density. *Annals of Botany* **118**(4): 685-698.

Radjai F, Wolf DE, Jean M, Moreau J-J. 1998. Bimodal character of stress transmission in granular packings. *Physical Review Letters* **80**(1): 61.

Ruiz S, Capelli A, van Herwijnen A, Schneebeli M, Or D. 2017. Continuum cavity expansion and discrete micromechanical models for inferring macroscopic snow mechanical properties from cone penetration data. *Geophysical Research Letters* **44**(16): 8377-8386.

Rutherford R, Gallois P, Masson PH. 1998. Mutations in *Arabidopsis thaliana* genes involved in the tryptophan biosynthesis pathway affect root waving on tilted agar surfaces. *The Plant Journal* **16**(2): 145-154.

Schindelin J, Arganda-Carreras I, Frise E, Kaynig V, Longair M, Pietzsch T, Preibisch S, Rueden C, Saalfeld S, Schmid B. 2012. Fiji: an open-source platform for biological-image analysis. *Nature Methods* **9**(7): 676-682.

Schneebeli M, Pielmeier C, Johnson JB. 1999. Measuring snow microstructure and hardness using a high resolution penetrometer. *Cold Regions Science and Technology* **30**(1): 101-114.

Sharpe J, Ahlgren U, Perry P, Hill B, Ross A, Hecksher-Sorensen J, Baldock R, Davidson D. 2002. Optical projection tomography as a tool for 3D microscopy and gene expression studies. *Science* **296**(5567): 541-545.

Silverberg JL, Noar RD, Packer MS, Harrison MJ, Henley CL, Cohen I, Gerbode SJ. 2012. 3D imaging and mechanical modeling of helical buckling in *Medicago truncatula* plant roots. *Proceedings of the National Academy of Sciences* **109**(42): 16794-16799.

Uga Y, Sugimoto K, Ogawa S, Rane J, Ishitani M, Hara N, Kitomi Y, Inukai Y, Ono K, Kanno N. 2013. Control of root system architecture by DEEPER ROOTING 1 increases rice yield under drought conditions. *Nature Genetics* **45**(9): 1097-1102.

Wendell D, Luginbuhl K, Guerrero J, Hosoi A. 2012. Experimental investigation of plant root growth through granular substrates. *Experimental Mechanics* **52**(7): 945-949.

White RG, Kirkegaard JA. 2010. The distribution and abundance of wheat roots in a dense, structured subsoil–implications for water uptake. *Plant, Cell & Environment* **33**(2): 133-148.

Whiteley GM, Dexter AR. 1982. Forces required to displace individual particles within beds of similar particles. *Journal of agricultural engineering research* **27**(3): 215-225.

Figures

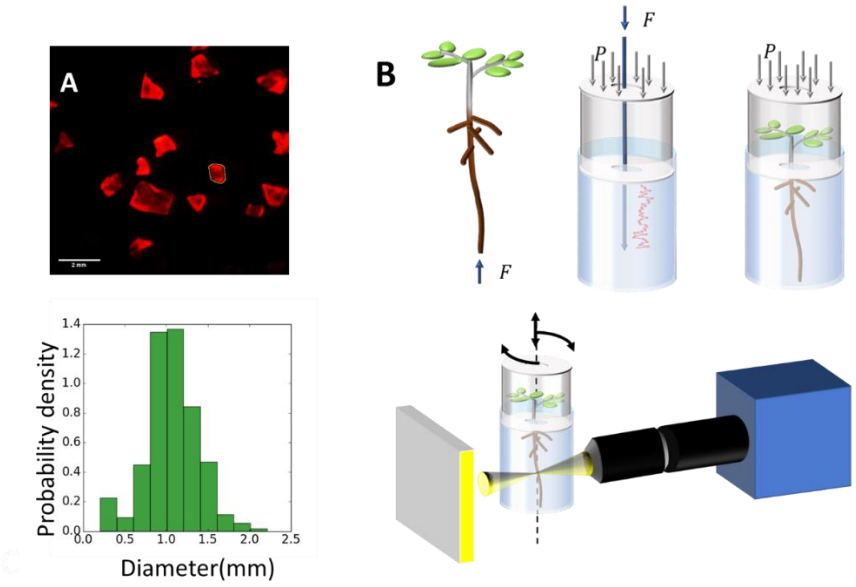

Figure 1. Experimental system for the study of root trajectories in response to soil particle forces. A) Transparent Soils are used as soil analogue. Stained particles can be used for visualisation and here also to quantify particle size distribution. The histogram of particle size distribution (below) shows particles have an average diameter of 1.07 mm ±0.32. B) Biomechanical analysis of root soil interactions is based on three experiments. First the buckling of root tips in compression was characterised on living root tips using a universal test frame (left). Measurements and control of particle forces were obtained from plants growing in a cylindrical chamber with the Transparent Soil maintained under controlled mechanical pressure using a piston fitted with a load cell (Methods S1). The transparent piston has a 3 mm opening to (i) monitor changes in particle forces using a penetrometer needle (middle) and (ii) to allow for emergence of the shoot (right). B) An optical projection tomography system with two degrees of freedom (rotation and vertical translation) is used to image the roots over large fields of view. The microscope assembles 720 projections of a root taken every 0.5 degree and at three depths.

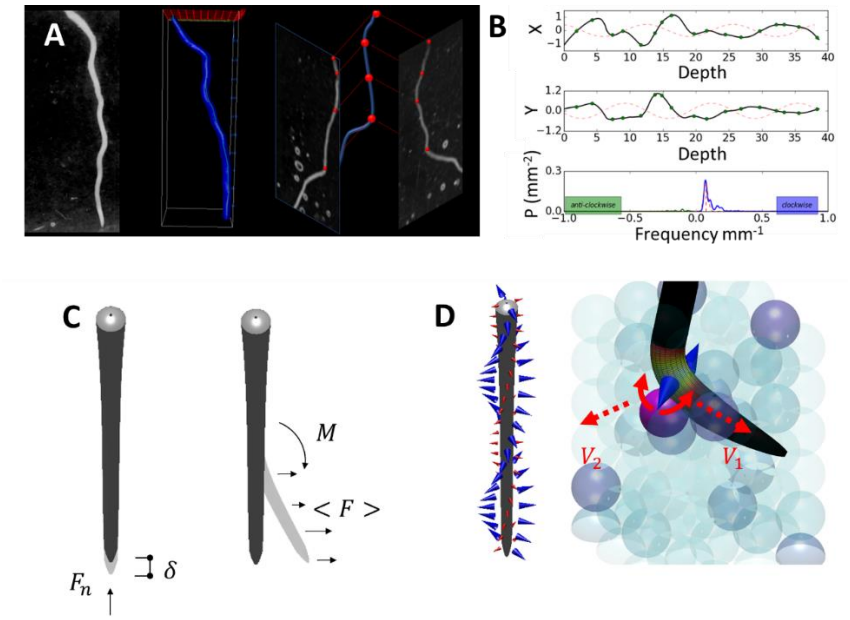

Figure 2. Pipeline for mechanistic understanding of root growth trajectories. A) The morphology of the root is characterised using a 3D image processing pipeline. (left) projection data are assembled by stitching followed by 3D reconstruction using the filtered back projection algorithm. A coarse representation of the centreline is first obtained using automated tracing (centre) and fine mapping of the root centreline is then obtained using multiplane tracing (right). B) Signal processing tools were developed to mine for local deflection of the root and detect helical waveforms. Here the root trajectory is projected in the XZ (top) and YZ (middle). The helical transform then provides the power spectrum of spatial frequency of the helical waveforms (bottom). The curve in red indicates the dominant wavelength waveform extracted by the study. A theory is also developed to understand root responses to soil particle forces. C) The theory considers two response modes. First, the root may overcome the resistance F of the particle resisting straight elongation (left). When F reaches a critical value, bending $\langle M \rangle$ and lateral displacement of particles $\langle F \rangle$ offer less resistance and a deflection occurs. D) Because a root has inherent helical anisotropy (principal axis of rotation as blue arrows, minor axis of rotations shown as red arrows), deflection occurs in the 3-dimensional space where two directions of deflections of least resistance V_1 and V_2 are equally probable. The sense of direction of the deflection is then determined by other biological factors.

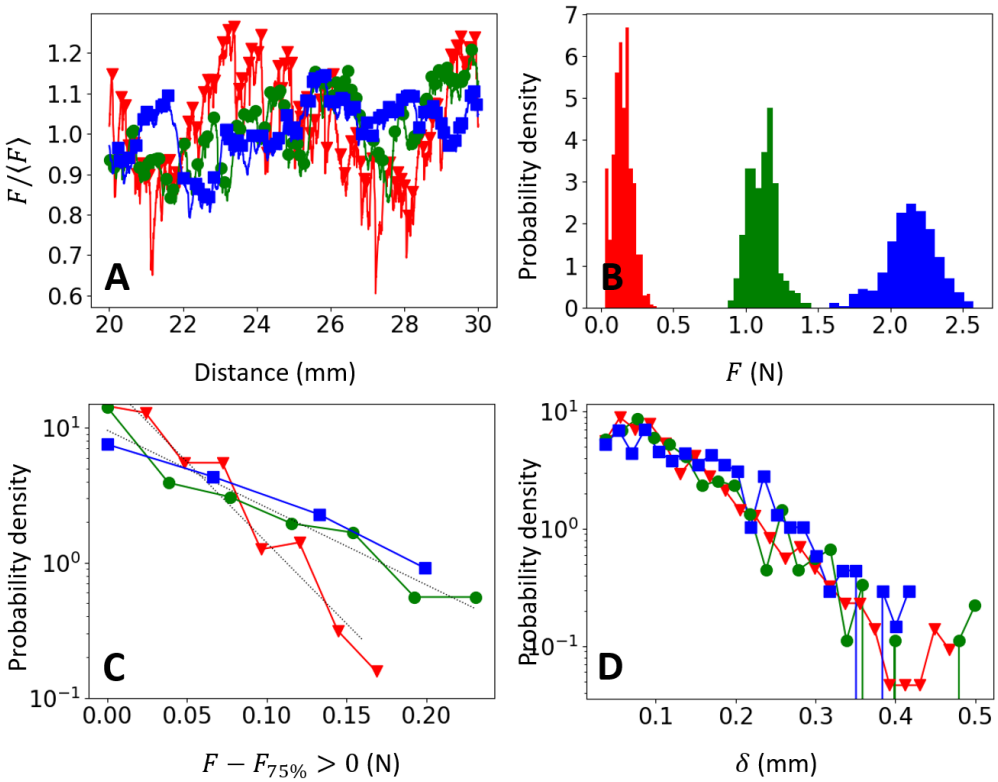

Figure 3. Granular physics of Transparent Soil. A) Variation in the force F(N) resisted by a penetrometer cone of similar size to a root (1.72 mm diameter) for different levels of confining pressure and measured at depths between 20 mm and 30 mm. The forces have been normalized by the averaged force $\langle F \rangle$ obtained over a travelled distance of 20 mm. The averaged force increases with confining pressure P. The markers indicate local maxima of the forces at different confining pressure (red triangle 0 kPa, green circle 25 kPa and blue square 50 kPa). To avoid sensitivity to sensor noise, only maxima that are absolute on a neighbourhood of 30 µm are identified. B) Probability density distribution of the forces (red triangle 0 kPa, green circle 25 kPa and blue square 50 kPa). C) Tail of the probability distribution of particle forces shows exponential decline, where $F_{75\%}$ is the third quartile. D) Probability density distribution of the distance between identified of forces F (markers in A) with red triangle 0 kPa, green circle 25 kPa and blue square 50 kPa.

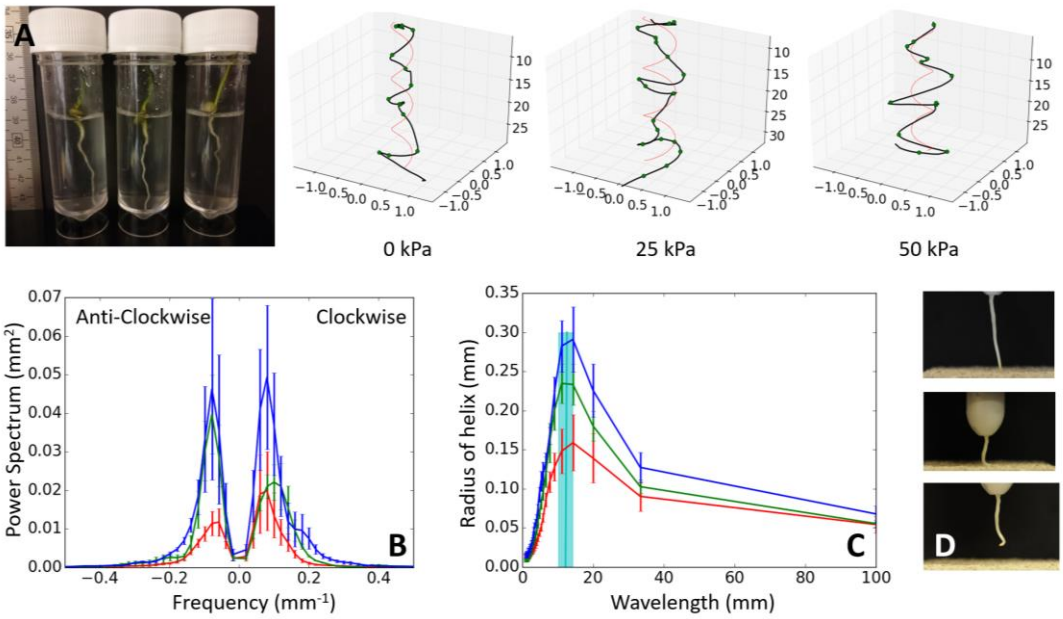

Figure 4. A) Lentil seedlings grown at increasing levels of confining pressure (from left). Typical centrelines (black curves) of roots grown under increased confining pressure (right). The horizontal X-Y coordinates are multiplied by 4 to enhance visibility. Markers indicate the sites of local maxima in root curvature and red lines show the dominant helix obtained by helical transform. B) The power spectrum of the helical transform from roots grown at respectively 0 kPa (red), 25 kPa (green) and 50 kPa (blue) shows helices can be both clockwise and anti-clockwise. C) Radius of the helical waveforms is influenced by the pressure from the soil respectively (same colour code as above) but the wavelength $\tilde{\lambda}$ is conserved at approximately 13 mm of root length. D) Root deformations in response to compression forces and buckling also exhibit helical patterns. The wavelength of the helix observed in these roots (12 mm) closely matched those grown in soil and is shown in cyan in figure (C) as a vertical line and a surrounding shadow indicating the confidence interval.

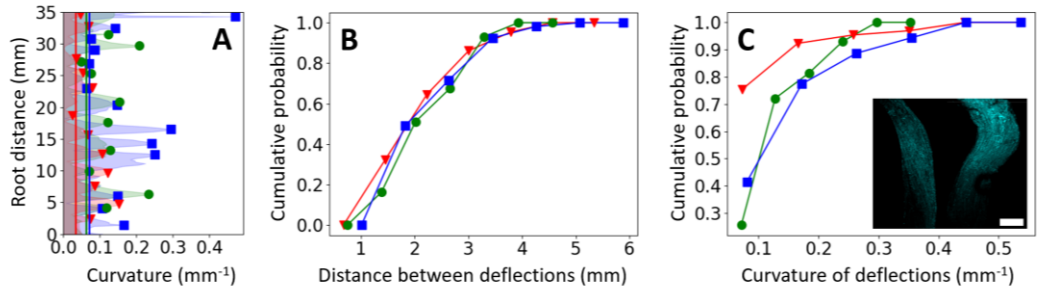

727

728 Figure 5. Development in granular media induces microscale deflections of the growth
729 trajectory. A) The profile of root curvature along the root (shaded area) shows that the
730 overall growth trajectory of the root is dominated by a sequence of local changes in
731 direction. The sites of deflections (markers) have high curvature with comparison to
732 the expected curvature from the global helix (vertical lines). B) The frequency of
733 deflections expressed as the distribution of the distance between the sites of two
734 consecutive deflections. The frequency follows an approximate uniform distribution
735 and is not influenced by soil confining pressure. C) The curvature at the site of the
736 deflection is increased with the soil confining pressure. Observations made with a
737 Confocal Laser Scanning Microscope shows localised bending of the root, here under
738 25 kPa and 50 kPa (bottom left, scale bar 500 µm). Red, green, and blue markers
739 indicate confining pressures of the Transparent Soil, respectively 0 kPa, 25 kPa and
740 50 kPa.

741

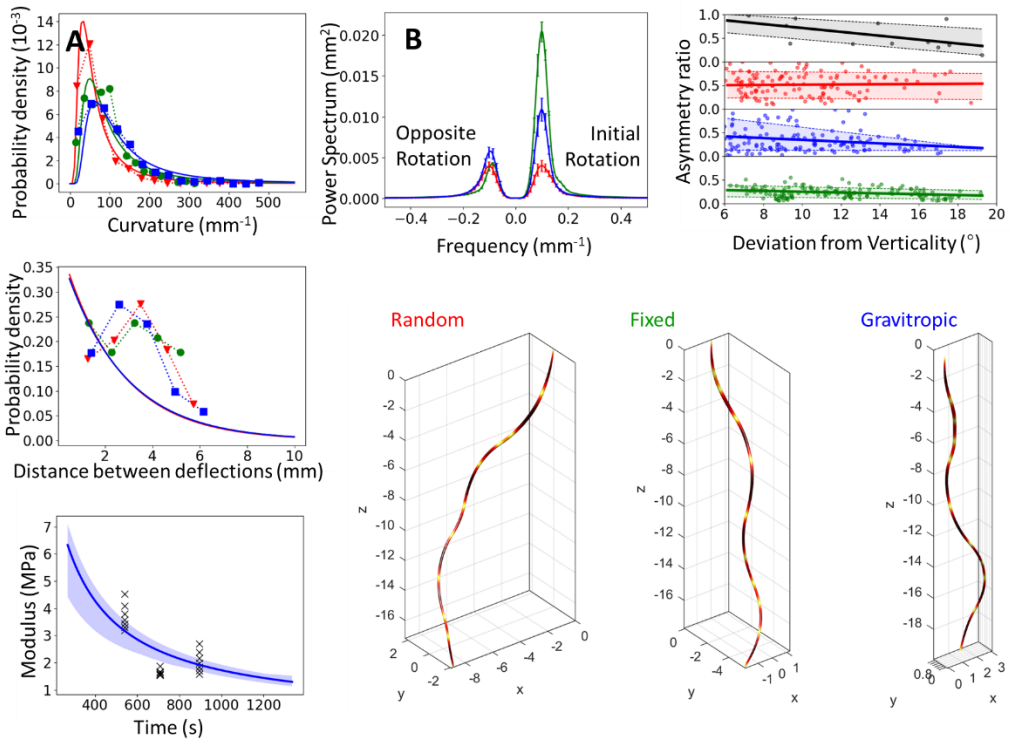

Figure 6. Predictions of root responses to particle forces. A) The theory predicts occurrence and magnitude of deflections, linking the distribution of root curvatures (top) and the frequency of occurrence of deflections (middle) to critical particle force, particle size and mean particle force. Suitable prediction can only be achieved with relaxation of the root stiffness with time, here modelled with the Kelvin Voigt viscoelastic model (bottom). Experimental data is plotted with dotted lines and theoretical predictions are plotted with plain lines. Red, green, and blue markers indicate confining pressures of respectively 0 kPa, 25 kPa and 50 kPa. B) Experiments and simulations showed gravitropic response is also required to obtain realistic 3-dimensional root trajectories, with both helical transform analysis (top) and visualisation (bottom) showing the effect of gravitropism in the formation of helices. Experimental data (black) shows the asymmetry ratio is influenced by deviation from verticality which confirms the role of gravitropism in the formation of helical patterns. Simulations of trajectory with random deflection (q_2=0.5, red) leads to large deviation from verticality and do not form dominant helical waveforms. When the sense of rotation is fixed (q_2=1, green), helical patterns are formed but deviations from verticality are observed. When root deflection is gravitropic (equation 11, blue) helices are formed with switches from clockwise to anticlockwise rotations. Plain lines were obtained by linear regression and shaded areas indicate the prediction intervals.